Journal of Catalysis 279 (2011) 144–154

Contents lists available at ScienceDirect

Journal of Catalysis

journal homepage: www.elsevier.com/locate/jcat

Mechanistic insights into the formation of acetaldehyde and diethyl ether from ethanol over supported VO_x, MoO_x, and WO_x catalysts

Hari Nair [a], Joseph E. Gatt [a], Jeffrey T. Miller [b], Chelsey D. Baertsch [a,*]

[a] School of Chemical Engineering, Purdue University, 480 Stadium Mall Drive, West Lafayette, IN 47907, USA
[b] Argonne National Laboratory, CSE, 9700 S. Cass Ave., Argonne, IL 60439, USA

ARTICLE INFO

Article history:
Received 22 August 2010
Revised 11 January 2011
Accepted 12 January 2011
Available online 22 February 2011

Keywords:
Vanadium oxide
Molybdenum oxide
Tungsten oxide
Anaerobic titration
Support effects
Ethanol oxidative dehydrogenation
Ethanol condensation
Ethanol dehydration
Reaction mechanism

ABSTRACT

Catalytic pathways are described for reactions of ethanol to acetaldehyde by oxidative dehydrogenation and of ethanol to diethyl ether by condensation over VO_x—Al_2O_3, MoO_x—Al_2O_3, and WO_x—Al_2O_3. Isotopic labeling shows that acetaldehyde formation occurs via rate-determining C—H bond cleavage of the CH_2 group in an adsorbed alkoxide followed by removal of surface oxygen in a Mars and van Krevelen redox mechanism (as confirmed by in situ X-ray absorption, diffuse reflectance infra-red Fourier transform spectroscopy and UV–visible spectroscopy); diethyl ether formation occurs in parallel via coupling and condensation of two adjacent ethoxy species. Using a combination of in situ spectroscopic and kinetic analysis, catalyst properties influencing the formation of acetaldehyde and ether from the common adsorbed ethoxy intermediate are elucidated. X-ray absorption analysis during anaerobic ethanol titration is used to preclude the involvement of terminal M=O bonds during the reaction. A study of the activity of catalysts with the same MoO_x domain size on Al_2O_3, TiO_2, and CeO_2 supports and binary oxides of MoOx and WO_x on Al_2O_3 are used to prove that the active redox oxygen for acetaldehyde formation is the oxygen atom linking the active metal oxide domain to the support oxide. Ether formation ability of the metal oxide is related to the electronegativity of the active metal atom.

© 2011 Published by Elsevier Inc.

1. Introduction

Catalysts containing redox-active metal oxides of V, Mo, Cu, and Ce, among others, are useful for the commercial production of acetaldehyde and acetic acid from ethanol via oxidative dehydrogenation processes (ODH). Alcohol ODH reactions are also useful as probe reactions for identifying the nature and density of active sites in nanostructured metal oxide catalysts [1–19].

While a large amount of literature is available describing methanol oxidative dehydrogenation over metal oxide catalysts [1,2,4,6,13] and alkane oxidative dehydrogenation [20,21], fewer studies have focused on reaction pathways using ethanol [12,22–24]. Methanol and ethanol ODH are believed to react through an alkoxide intermediate [12–15,25], and Oyama and Zhang have shown using silica-supported MoO_x catalysts that a monodendate ethoxide species actively participates in acetaldehyde formation [12]. Separate studies over supported molybdenum and vanadium oxide catalysts suggest that the rate-determining step is H-atom abstraction from the CH_2 group [12,14,22]; however, the universality of this mechanism for different transition metal oxides (both acidic and redox) has not been demonstrated. Further, the mechanism for ether formation has never been detailed with supporting evidence, though a number of feasible mechanisms have been proposed [9] including the condensation of multiple adsorbed species, the involvement of mono and bidendate species and mechanisms involving condensation of an adsorbed ethoxy species with vapor phase ethanol.

Of even greater importance, debate over the identity of the specific catalytically active oxide moiety responsible for alcohol oxidation reactions continues in the literature. Active sites have been proposed to consist of either the M=O, M—O—M or M—O-support structures (where M is an active transition metal atom) [26–31]. Ono et al. have also demonstrated the lack of activity of crystalline MoO_3 species and have related the rate of ethanol ODH to the strength of the Mo=O bond as obtained through infra-red spectroscopy studies and use this as a basis for crediting polymolybdate species for higher rates [32]. In contrast, Oyama and Somorjai [11] have shown that ethanol oxidation over silica-supported vanadia catalysts is structure independent if active site densities are measured using oxygen chemisorption, and our previous studies using ethanol as a probe molecule under anaerobic conditions also indicate that intrinsic turn-over rates do not change with the size of the oxide domain [33] in alumina-supported oxide catalysts of molybdenum, tungsten and vanadium. Recent work by Routray et al. using methanol temperature programmed surface reaction has demonstrated that there is no relation between the strength

* Corresponding author. Fax: +1 765 494 0805.
E-mail address: baertsch@purdue.edu (C.D. Baertsch).

0021-9517/$ - see front matter © 2011 Published by Elsevier Inc.
doi:10.1016/j.jcat.2011.01.011

of the terminal M=O bond and the activity of molybdates and vanadates for methanol oxidation [34]. Other work from the same group have shown that the CH_3OH oxidative dehydrogenation kinetic parameters are independent of the surface bridging V—O—V bond concentration surface V=O bond length/strength and vanadium surface density on the alumina support [35]. Work in this group has also been directed toward understanding the root of acidity in supported tungsten oxide catalysts [36,37]. However, the factors influencing acidic and redox activity on the same catalyst are still not clear and have not been addressed by too many studies.

Thus, considerable debate remains regarding the mechanism of ethanol oxidation on metal oxide catalysts and also the effect of catalyst structure and composition on ethanol ODH rate and selectivity. This study aims to detail the mechanism of ethanol oxidative dehydrogenation and dehydration over alumina-supported molybdenum, tungsten, and vanadium oxide catalysts. We propose mechanisms for the formation of both acetaldehyde and diethyl ether from ethanol. Supporting evidence for these mechanisms based on isotope experiments, in situ ultraviolet–visible diffuse reflectance spectroscopy (UV–vis DRS), in situ diffuse reflectance infra-red Fourier transform spectroscopy (DRIFTS), and X-ray absorption spectroscopy is shown. Anaerobic titrations using ethanol, which we have previously used to identify the number of active redox sites on supported metal oxide catalysts [33], are used in conjunction with these spectroscopic techniques to obtain additional information on the site requirements for ethanol oxidation. Through the use of binary oxide catalysts and different supports, we also demonstrate the role of oxygen linkages between the metal and the support in the formation of acetaldehyde. The catalytic properties influencing redox (acetaldehyde) and acid (ether) product formation are also hypothesized based on these studies.

2. Experimental methods

2.1. Catalyst preparation

Alumina-supported catalysts containing tungsten oxide (WO_x—Al_2O_3), molybdenum oxide (MoO_x—Al_2O_3), vanadium oxide (VO_x—Al_2O_3), and binary mixtures of two transition metal oxides (MoO_x/WO_x—Al_2O_3) with surface densities varying from 0.5 to 8 metal atoms/nm^2 were prepared by incipient wetness impregnation of γ-alumina (Alcoa 151 m^2/g, 98.8%) with aqueous solutions of ammonium tungsten oxide ($(NH_4)_{10}W_{12}O_{41}\cdot 5H_2O$, Alfa Aesar, 99.999%), ammonium molybdate ($(NH_4)_6Mo_7O_{24}\cdot H_2O$, Alfa Aesar, 99.999%), and ammonium vanadium oxide (NH_4VO_3, Alfa Aesar, 99.995%). Metal atom surface densities are based on the initial alumina surface area available for impregnation (151 m^2/g). BET results obtained by N_2 physisorption at 77 K on a Micromeretics ASAP 2000 confirm that the surface area does not decrease significantly at the surface densities studied here, as also shown in previous reports [28]. Catalysts were dried overnight at 393 K and then calcined in flowing air (zero grade, 0.5 cm^3/s) at 923 K (0.33 K/s) for 3 h. Catalysts containing a binary mixture of MoO_x and WO_x domains were prepared by impregnation with a solution containing both precursors (coimpregnation). Catalysts are referred to by the appropriate metal atom surface density and the metal itself – thus 2 W refers to a tungsten oxide catalyst with 2 W atoms per nm^2 of the support. It is recognized that the high calcinations temperature results in the formation of a $Al_2(MoO_4)_3$ in the case of supported MoO_x—Al_2O_3 catalysts, but this has no influence on the conclusions of this study.

The iron molybdate catalyst used in this study for the comparison of rate and selectivity over various alcohols was synthesized via co-precipitation of 2.3 M $Fe(NO_3)_3\cdot 9H_2O$ and 0.3 M $(NH_4)_6Mo_7O_{24}\cdot 4H_2O$ with an overall 2.0 Mo/Fe ratio in the solution. After thermal aging, the catalyst was dried at 343 K and calcined in flowing dry air at 673 K. The detailed synthesis and structural characterization of these catalysts is described by Gatt et al. [38]. Complete lists of catalyst properties can be found in the study by Nair et al. [39,38].

2.2. Ultraviolet–visible diffuse reflectance spectroscopy

Ultraviolet–visible (UV–vis) diffuse reflectance spectra (DRS) of prepared catalysts were obtained using a Varian (Cary 5000) spectrophotometer with a Harrick-Scientific Praying-Mantis diffuse reflectance accessory (DRA) and in situ cell (HVC-DRP). Data were collected by linear scanning in units of cm^{-1} over the range of 3500–50,000 cm^{-1}. All samples were ground before measurements, and magnesium oxide was used as a reflectance reference. Reported spectra were taken at room temperature without any prior treatment. In situ oxidation/dehydration at 773 K in flowing dry air for an hour had no effect (within the measurement limits of ±0.2 eV) on absorption edge energies, similar to previous reports [30]. In situ spectra were collected over about 0.030 g of catalyst in the high temperature in situ cell over the range of 3500–50,000 cm^{-1}. All samples were pretreated in 1.67 cm^3/s of simulated air (22% O_2/He) at 573 K for 1 h and then exposed to the reaction mixture consisting of ethanol (0.5 mol%), O_2 (1.5 mol%) and balance He. A Cole Palmer single-syringe infusion pump (EW-74900-00) was used to inject ethanol into the flow of O_2 and He. Gases passed through the catalyst bed, and temperature was measured using a thermocouple immediately below the bed.

2.3. Alcohol reactions

Steady-state reactions were conducted in a continuous flow, fixed bed, vertical U-tube quartz reactor containing 0.022–0.044 g of 125–250-μm particle catalyst dispersed on a quartz frit. Temperature was measured using a thermocouple placed within a groove situated approximately 2 mm above the catalyst bed. All samples were pretreated in 1.67 cm^3/s of simulated air (22% O_2/He) at 773 K for 2 h in order to eliminate any moisture on the surface and to ensure complete oxidation and then allowed to cool to reaction temperature. Liquid ethanol (0.022–0.05 cm^3/s, AAPER, absolute 200 proof) was vaporized into a flowing mixture of oxygen and helium by controlled injection with a Cole Palmer single-syringe infusion pump maintaining a constant partial pressure of 0.5 kPa ethanol in 1.5 kPa oxygen. Methanol (Sigma Aldrich, anhydrous 99.8%), 1-propanol (Sigma Aldrich, anhydrous 99.7%), 2-propanol (Alfa Aesar, anhydrous 99.5%), 1-butanol (Alfa Aesar, Ultrapure 99.0%), and 2-butanol (Alfa Aesar, Ultrapure, 99.0%) were injected similarly into the gas stream. Water addition was accomplished by mixing water with ethanol in the desired ratio (0–100 mol% ethanol) and injecting the mixture using the syringe pump. Reactant and product concentrations were measured using an Agilent 6890GC with FID and TCD detection (HP-PLOT Q column). All reactions were carried out at 453 K with total gas flow rates between 0.83 and 1.83 cm^3/s. No conversion was observed at 453 K with a blank reactor and no catalyst deactivation was observed. Conversion is reported as the moles of ethanol reacted per mole of ethanol fed. Product selectivity was found to be independent of conversion under the range of conversions studied (indicating that there is no interconversion of the products) and is reported as the moles of a particular product formed per mole of all products formed at 0% conversion.

Anaerobic reactions were carried out as described in previous work [27]. Briefly, steady-state reaction was obtained through the procedure outlined earlier. The oxygen in the gas phase was then cutoff, and acetaldehyde formation and ether formation were

simultaneously monitored using a combination of a Hiden Analytical HPR20 mass spectrometer and an Agilent 3000A microGC (PLOT Q column). Quantification of the acetaldehyde formed after oxygen cutoff was used to determine the number of active redox sites.

2.4. Diffuse reflectance infra-red Fourier transform spectroscopy

In situ diffuse reflectance infra-red Fourier transform spectroscopy (DRIFTS) data were collected with a Nicolet Magna-860 spectrometer using a Harrick Scientific Praying Mantis diffuse reflectance accessory (DRA) and in situ reaction cell (HVC-DRP). Spectra were averaged over 128 scans with a resolution of 4 cm^{-1} and mirror velocity of 1.8988 cm s^{-1}. Approximately 0.030 g of powdered catalyst was loaded into the reaction cell and supported on a horizontal quartz frit. Gases were mixed upstream and passed downward through the catalyst bed. Temperature was measured and controlled by a thermocouple immediately beneath the catalyst bed. A background spectrum was collected at reaction temperature after pretreatment in 10% O_2 balance He at 773 K and used to convert reflectance measurements into absorbance units. The region of the spectra in the range 2800–3100 cm^{-1} was fit with four Gaussian peaks that are characteristic of adsorbed ethoxy species. Fitting and quantification of the area under the peaks was performed using the commercially available CasaXPS software.

2.5. X-ray absorption spectroscopy

Mo K and W L_{III} edge EXAFS and XANES data were collected on the insertion-device beam line of the Materials Research Collaborative Access Team (MRCAT, Sector 10 ID) at the Advanced Photon Source, Argonne National Laboratory. A cryogenically cooled double-crystal Si (1 1 1) monochromator was used in conjunction with an uncoated glass mirror to minimize the presence of harmonics. The monochromator was scanned continuously during the measurements with data points integrated over 0.5 eV for 0.07 s per data point. Measurements were made in transmission mode with the ionization chambers optimized for the maximum current with linear response ($\sim 10^{10}$ photons detected s^{-1}) using a mixture of N_2 and He in the incident X-ray detector and a mixture of ca. 20% Ar in N_2 in the transmission X-ray detector. A Mo (or W) foil spectrum was acquired simultaneously with each measurement for energy calibration.

In situ spectra were collected by heating the samples to desired temperatures and mimicking reaction conditions described for ethanol oxidation and anaerobic titrations using mass flow controllers as far as possible. Ethanol was introduced into the vapor phase using an ice-cooled saturator through which air was passed. Catalysts were pressed into a pellet within a hollow cylindrical stainless steel tube placed inside a quartz tube slightly larger than the inner tube. The entire arrangement was sealed with Kapton windows and placed lengthwise along the direction of the beam. Heating was achieved by a thermal jacket around the quartz tube, and temperature was monitored using a thermocouple inside the tube. Ethanol was introduced using a saturator in an ice bath at 273–278 K providing 1.5–3 kPa of ethanol in He and O_2 which passed through the tube and catalyst bed. Due to the variations in experimental setup, comparison of absolute values with experiments in the laboratory is not done, and hence, trends are compared instead. Some by-passing of the pellet is believed to occur in the XAS setup, the effect of which is evident in results described later.

Analysis of X-ray absorption spectra including Fourier transform analysis and spectra fitting were performed using the WINXAS software. Background subtraction was performed by fitting linear polynomials to the pre-edge and 3rd degree polynomials to the post-edge region. The XANES spectra incorporated the range 10.15–10.24 keV for W catalysts and standards and 19.97–20.06 keV for Mo catalysts and standards. The pre-edge and total XANES spectra were fit using a linear combination of standard compounds, sodium molybdate (Na_2MoO_4), ammonium heptamolybdate ($(NH_4)_6Mo_7O_{24}$), and molybdenum oxides (MoO_2 and MoO_3) to gain insight into the coordination and the oxidation state of the Mo atoms in the catalyst. The XANES spectra of the reduced catalysts were fit using a linear combination of MoO_2 (Mo oxidation state + 4) and MoO_3 (Mo oxidation state + 6). This fitting was done for the position and slope of the absorption edge, while excluding the pre-edge and the features after the edge. The fitting was done in the region between 0.1 and 0.8 times the step height. The relative amounts of MoO_2 and MoO_3 that gave the best fit were used to calculate the final oxidation state.

The EXAFS spectra were obtained extracted using cubic splines to obtain a smooth background. The radial distribution function was obtained by taking the Fourier transform of the k^2 weighted chi function (Δk = 2.8–10.5 $Å^{-1}$ for Mo compounds and Δk = 2.7–10.6 $Å^{-1}$ for W compounds). Fitting of the EXAFS spectra was performed using the WINXAS software. Supported Mo oxides catalysts contain a variety of bond lengths making fitting of the EXAFS not, generally, possible. However, since the amount of reduced Mo in the reduce catalysts, i.e., anaerobic titrations, was small and assuming that the structure of the unreduced Mo is little changed, the EXAFS of the difference spectra (oxidized minus reduced catalyst) represents the structure of the reduced Mo—O bonds. The first shell fit of the Mo—O EXAFS of the difference spectrum gives the coordination number and bond distance of the catalytic Mo. Briefly, the fitting started with fixing the Debye Waller Factor (DWF) at 0.002 for oxides and fitting *N* (coordination number), *R* (bond distance), and Eo (absorption edge energy). The Mo—O phase and amplitude functions used for the fitting were prepared from the isolated first shell Mo—O peak of Na_2MoO_4 (4 Mo—O at 1.77 Å). The sensitivity toward DWF changes was determined by changing the DWF from 0.001 (too low) to 0.005 (too high) and looking at the changes in other free parameters. The changes in *N* for the difference Mo—O were less than 0.1 (out of 0.4) in *N*, 0.01 in *R* and less than 1 in Eo. The best fit with DWF was chosen for the bond distance *R*.

3. Results

3.1. Ethanol reaction characterization

Ethanol ODH reactions over alumina-supported VO_x, MoO_x, and WO_x catalysts at 453 K result in two products – acetaldehyde and diethyl ether. No other products were observed at 453 K. Formation of acetaldehyde indicates the presence of redox sites on the catalyst, while diethyl ether formation indicates the presence of acid sites on the catalyst [6]. Product formation rates per metal atom are shown for MoO_x—Al_2O_3, VO_x—Al_2O_3 and WO_x—Al_2O_3 catalysts as a function of surface density in Fig. 1 (data previously reported in [33]). As has been reported previously, oxides of vanadium and molybdenum are redox in character, with higher production rates for acetaldehyde, while tungsten oxide has significant acidic character and produces mainly diethyl ether [3,5,6,40–42] (Fig. 1c). Diethyl ether formation rates per metal atom decrease continuously with increasing surface density, while acetaldehyde rates show a slight maximum at surface densities reported near monolayer coverage for molybdenum and vanadium oxide catalysts [43–46]: 4 metal atoms/nm^2 for Mo and 8 metal atoms/nm^2 for V. In the case of the supported tungsten oxide catalysts, the acetaldehyde formation rates are low, and hence, it is difficult to discern a maximum rate. As is clear from Fig. 1, surface density has a significant effect on both product formation rates and

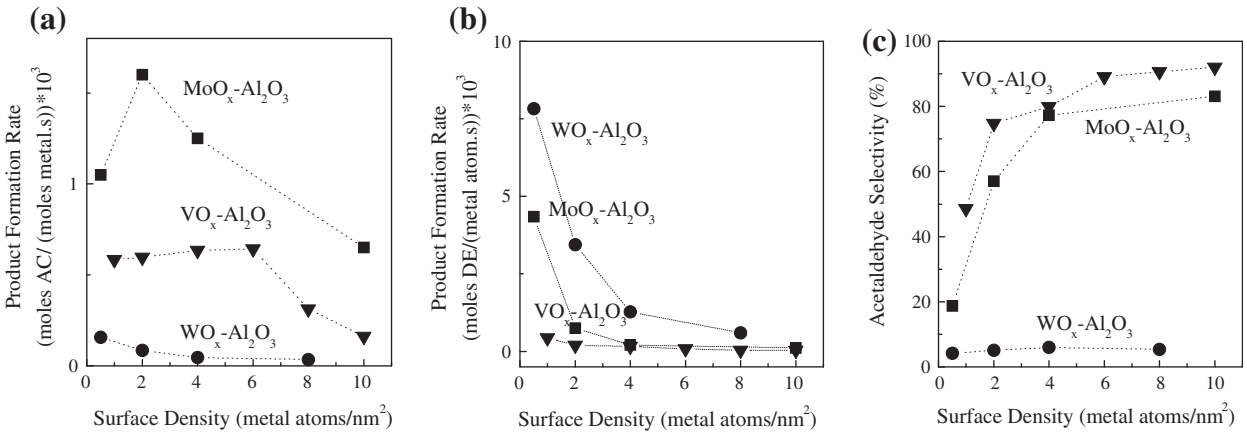

Fig. 1. Rates of formation (per metal atom) for (a) acetaldehyde (some data reproduced from [27]), and (b) diethyl ether and acetaldehyde selectivity (c) as a function of surface density for MoO_x—Al_2O_3, VO_x—Al_2O_3 and WO_x—Al_2O_3 catalysts.

acetaldehyde selectivity. Our previous studies have shown that the effect of surface density on acetaldehyde formation rate is due to a change in the number of accessible redox sites [33] with surface density and that the redox properties and exposed alumina variations with surface density affect the acetaldehyde selectivity [39]. This study focuses on combining such knowledge with mechanistic studies to obtain a more complete relationship between catalyst properties, rate, and in particular selectivity trends as seen in Fig. 1c. All mechanism studies were carried out using catalysts with monolayer coverage to minimize support effects.

The dependence of the ethanol ODH rate over 8V on ethanol and oxygen concentrations was investigated (data not shown). Absolutely no variation in the ethanol ODH rate is seen with either 0.25–2.0 mol% ethanol or 1.5–5.0 mol% oxygen. The zero-order rate dependency on ethanol concentration is consistent with a Langmuir–Hinshelwood type mechanism where the oxide surface is saturated with reactive ethanol intermediates at these concentrations and suggests that the first step in the ethanol ODH mechanism is the adsorption of alcohol on the catalyst surface. The absence of any effect of oxygen concentration on the oxidation rate suggests that oxidation occurs either through chemisorbed oxygen or through the Mars–van Krevelen redox mechanism.

3.2. In situ FTIR characterization

In situ FTIR was used to examine relative ethoxy coverages and species during reaction to aid in mechanism elucidation. Oyama and Zhang have observed two types of chemisorbed ethoxy species for molybdenum oxide on silica – one associated with terminal Mo═O bonds and the other with bridging Mo—O—Mo bonds [12]. A typical DRIFTS spectrum collected over alumina-supported VO_x, MoO_x, and WO_x catalysts during ethanol oxidation at 453 K is shown in Fig. 2a. As shown in Fig. 2b, four peaks can be deconvoluted in the region between 2870 and 2975 cm^{-1} and can be attributed to adsorbed ethoxy species [12]. Vibrations at ~2972 and 2928 cm^{-1} have been attributed to the CH_3 group and peaks at ~2872 and 2892 cm^{-1} to vibrations associated with the CH_2 group in the monodendate species (CH_3CH_2O—M) and bidendate species with an ethoxy species coordinated to two metal atoms (CH_3CH_2O—M_2), respectively, where M represents the metal atom. These peaks are shifted in our spectra. In our data, the combined area under peaks at 2882 (monodendate) and 2902 cm^{-1} (bidendate) includes the vibrations due to both types of adsorbed species and is used to obtain an estimate for the total ethoxy coverage. Both monodendate and bidendate ethoxy species are seen irrespective of whether the dominant product is acetaldehyde or diethyl ether, indicating that the ethanol adsorption step is common to the formation of both products and that both types of adsorbed species are observed irrespective of the redox/acidic nature of the catalyst. No trends were observed in the ratio of the monodendate to bidendate species with the type of catalyst used. Also, all variations in the areas associated with either monodendate or bidendate species mimic those observed with the total ethoxy area; thus, for further analysis, any of these relative areas can be used interchangeably.

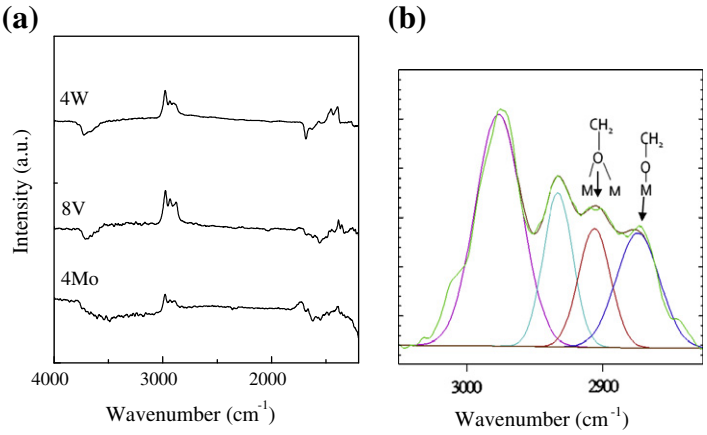

Fig. 2. (a) DRIFTS spectrum collected over a 4W, 8V and 4Mo catalyst under steady-state ethanol oxidation at 453 K. (b) Deconvolution of peaks corresponding to ethoxy species on the catalyst surface during ethanol oxidation over a 4Mo catalyst.

Ethoxy coverage was varied by adding water to the reactant stream (at a constant ethoxy partial pressure of 0.05 MPa) and monitored by FTIR during reaction with ethanol over the 8V catalyst as shown in Fig. 3a. Spectra collected during steady-state ethanol reaction (with no water in the feed) were used as background references for absorbance spectra during reaction with water, and relative coverages are shown in Fig. 3a. As seen by the decreased area of all four ethoxy peaks upon introduction of water, it is clear that water adsorbs on active catalytic sites, displacing ethoxy species and decreasing ethoxy coverage with increasing water/ethanol ratios in the feed.

The dependence of product formation rates on ethoxy coverage can then be examined using these experiments. Product formation rates were measured in a plug-flow reactor using identical water/ethanol mixtures to mimic the in situ FTIR studies for both a mainly redox catalyst (8V) and a mainly acidic catalyst (4W). Rates in ethanol/water were normalized with product formation rates obtained in pure ethanol at 453 K. Normalized product formation rates are shown as a function of the fractional ethoxy coverage (relative to the coverage obtained at 453 K for only pure ethanol in the feed) for the 8V and 4W catalysts in Fig. 3b and c, respectively. Experimental variability resulted in a coverage value slightly larger than 1.0 during one experiment over the 8V catalyst – this is not chemically significant and only represents experimental error. For both catalysts, acetaldehyde formation rates follow a linear, first-order dependence on ethoxy species concentration and diethyl ether formation rates follow an apparent power-law dependence on the concentration of adsorbed ethoxy species. While this dependence is not clear based on the data over vanadium catalysts, it should be kept in mind that ether formation rates are extremely low in these catalysts. Changes in the ether rates (especially when large amounts of water are added in the feed) are, therefore, within error and are clearer in the data for the 4W catalyst. As has been mentioned earlier, the coverage of both monodendate and bidendate species show the same trends as the overall ethoxy species, and hence, no conclusion can be drawn as to the coordination of the adsorbed ethoxy species. It can be concluded though that acetaldehyde is formed through the transformation of a single ethoxide species (as indicated by the linear dependence on ethoxy coverage), and the formation of diethyl ether requires the interaction of multiple ethoxide species on the surface (as indicated by the non-linear dependence on ethoxy coverage).

As mentioned previously, the DRIFTS experiments do not conclusively demonstrate that either the monodendate or the bidendate species are responsible for acetaldehyde or ether formation. Additionally, it is possible to propose a number of competing mechanisms for the formation of both acetaldehyde and ether based on interactions of a monodendate/bidendate species with either another adsorbed species or a gas phase ethanol species [3,9,12]. However, only a few mechanisms result in rate expressions that satisfy the experimentally observed dependencies on both ethoxy coverage (first order for acetaldehyde and higher order for ether) and ethanol concentration (zero order for both). It was found that only mechanisms involving monodendate species could result in the observed dependencies – this also implies that the same sites are responsible for both acetaldehyde and diethyl ether, evidence for which will be presented later.

3.3. In situ UV–vis DRS characterization

The adsorption site for ethoxy species was further investigated using UV–vis diffuse reflectance spectroscopy. Fig. 4 compares the UV–vis DRS spectra for the 4Mo catalyst prior to and during reaction with ethanol at 453 K. Under ambient conditions and prior to reaction, a single absorption edge is seen at ~3.3 eV, characteristic of a polymeric MoO_x domain near monolayer coverage [33]. This absorption edge arises from electronic transitions from the highest occupied molecular orbital to the lowest unoccupied molecular orbital. Upon exposure to ethanol at 453 K, absorption begins at lower energies (~1.5–2 eV) in the visible portion of the spectrum

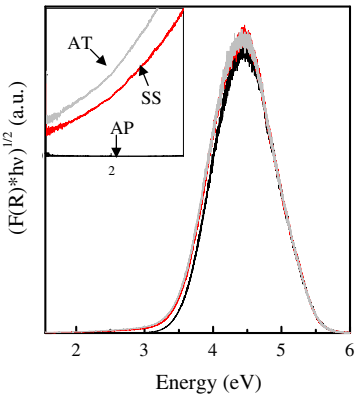

Fig. 4. UV–vis absorption spectra for 4Mo catalyst after pretreatment (AP), during steady-state ethanol oxidation at 453 K (SS) and after anaerobic titration (AT) at 453 K. A shift in the absorption edge energy is seen from 3.3 eV to ~3.2 eV after exposure to ethanol under reaction conditions. No significant change is seen after anaerobic titrations with ethanol. Inset shows an expansion of the region between 1.5 eV and 2.1 5 eV.

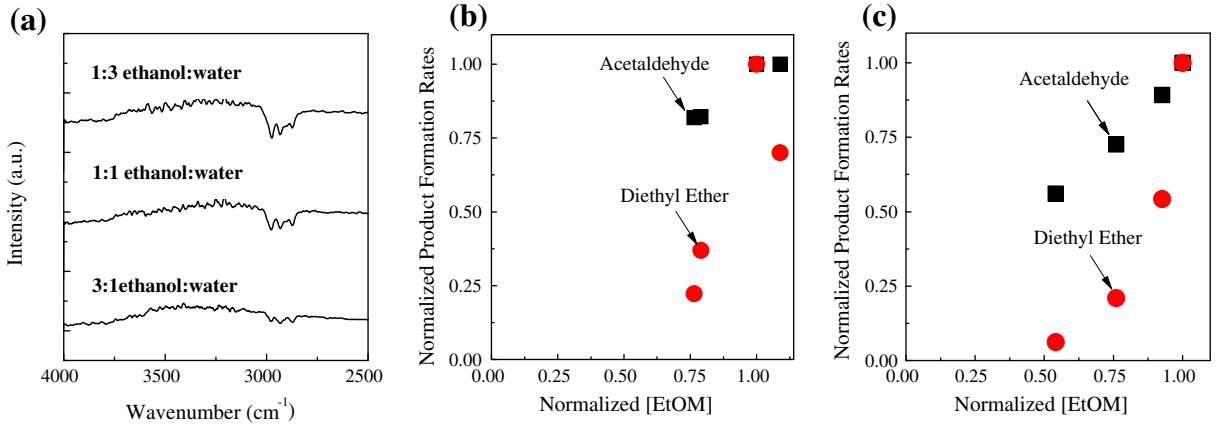

Fig. 3. (a) DRIFTS spectra collected over the 8V catalyst using a binary ethanol/water feed at 453 K at different ethanol:water feed ratios (total ethanol + water pressure constant at 0.5 kPa). Product formation rates normalized to the rate without water addition (0.5 kPa ethanol) at 453 K over the 8V catalyst (b) and the 4W catalyst (c) as a function of the relative ethoxy coverage.

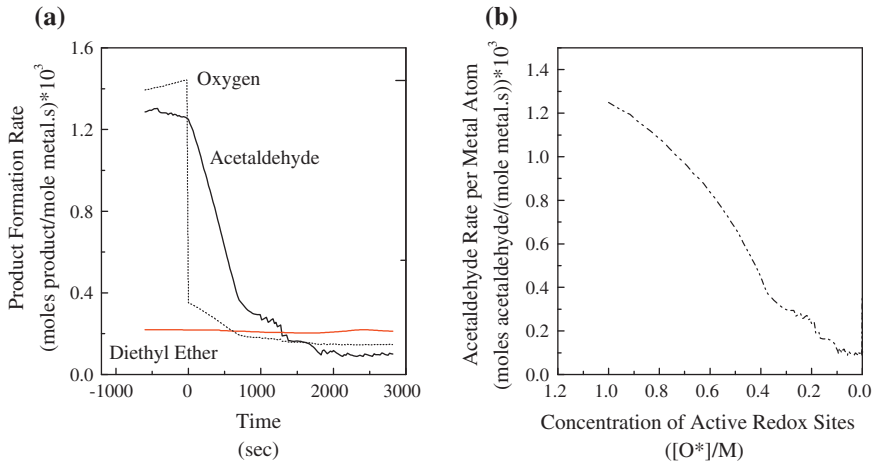

Fig. 5. (a) Product formation rates as a function of time during anaerobic titration in ethanol over 4Mo at 543 K and (b) acetaldehyde production rate over 4Mo as a function of the number of remaining active redox sites.

characteristic of d–d transitions in reduced Mo centers [41,47,48] and resulting in accordance with color changes in the sample, showing that ethanol adsorption occurs on the metal centers and is coincident with their reduction. Note that changes in edge energy are much distinct from those that occur due to domain size effects – while reduction results in an increase in absorption at energies much lower than the absorption edge energy (1.5–2 eV vs. > 3 eV), and domain size changes result in an actual shift of the absorption edge [41,49].

3.4. Anaerobic site titration

Anaerobic titrations using ethanol have previously been demonstrated for the quantification of active redox site densities in supported oxide catalysts [33]. Such measurements are accomplished by removing oxygen instantaneously during steady-state reaction and monitoring product formation rates. Upon oxygen removal, the acetaldehyde production rate drops in an exponential fashion as shown in Fig. 5a for the 4Mo catalyst, while ether production rates are not affected.

This behavior could result from oxidation mechanisms utilizing either chemisorbed oxygen or lattice oxygen (via a Mars–van Krevelen pathway). However, the UV–vis absorption spectrum collected during the anaerobic titration of 4Mo (Fig. 4b) shows an increase in the pre-edge absorption feature relative to steady-state reaction conditions, confirming that the catalyst surface reduces during the anaerobic titration. It is therefore clear that ethanol ODH to acetaldehyde proceeds with the removal of lattice oxygen. By quantifying the amount of acetaldehyde produced after oxygen cutoff, it is possible to compute the number of active sites or removable oxygen available on that catalyst for acetaldehyde formation under steady-state conditions, which is represented by the area under the acetaldehyde curve after oxygen removal (Fig. 5a). This active oxygen site density can be used to calculate an intrinsic redox turn-over rate, which as we have reported previously is the same for V, Mo, and W oxides supported on alumina independent of surface density [33]. As shown in Fig. 5b for the 4Mo catalyst, the acetaldehyde production rate varies linearly with the number of active redox sites remaining during the anaerobic titration – similar variations are observed for VO_x—Al_2O_3 and WO_x—Al_2O_3 catalysts (not shown). In situ DRIFTS analysis shows that the ethoxy coverage remains constant during anaerobic titration. Therefore, the decreasing rate results only in a loss of active sites and is not resultant from changes in ethoxy coverage.

The number of redox sites per metal atom is shown for different catalysts in Table 2. As shown in Fig. 1, acetaldehyde formation rates per metal atom depend on metal atom surface density, though we have previously shown that this variation is due to a change in the number of active redox sites rather than due to changes in the intrinsic rate of the active site. This information, along with the data in Table 1, lends some insight into the nature of the removable oxygen for acetaldehyde formation. As seen in Table 1, in each of the three oxides, the number of active sites per metal atom increases with increasing surface density until monolayer coverage, after which a decrease in the number of redox sites per metal atom is observed. This can now be compared to the relative amounts of the three types of oxygen atoms in these metal oxide surface structures – the terminal M=O oxygen, the bridging oxy-

Table 1
Number of active sites per metal atom for different Mo, W, and V oxide catalysts.

Catalyst	Active redox sites per metal atom
0.5Mo	0.97*
2Mo	1.18*
4Mo	1.30*
8Mo	1.13*
2W	0.05*
4W	0.03*
0.5V	0.80*
2V	0.72*
4V	0.74*
6V	0.71*
8V	0.64*
10V	0.16*
0.5Mo/0.5W	0.38
2Mo/2W	0.66

* Reported previously in [27].

Table 2
Acetaldehyde (AC) rates per metal atom and acetaldehyde selectivity for V oxide catalysts on different supports at 453 K.

Catalyst (edge energy)	AC rate × 10^3 (mol AC/metal atom-s)	AC selectivity (%)
2V Al_2O_3 (2.6 eV)	0.60	67
2V CeO_2 (2.5 eV)	5.83	100
2V TiO_2 (2.3 eV)	21.70	100

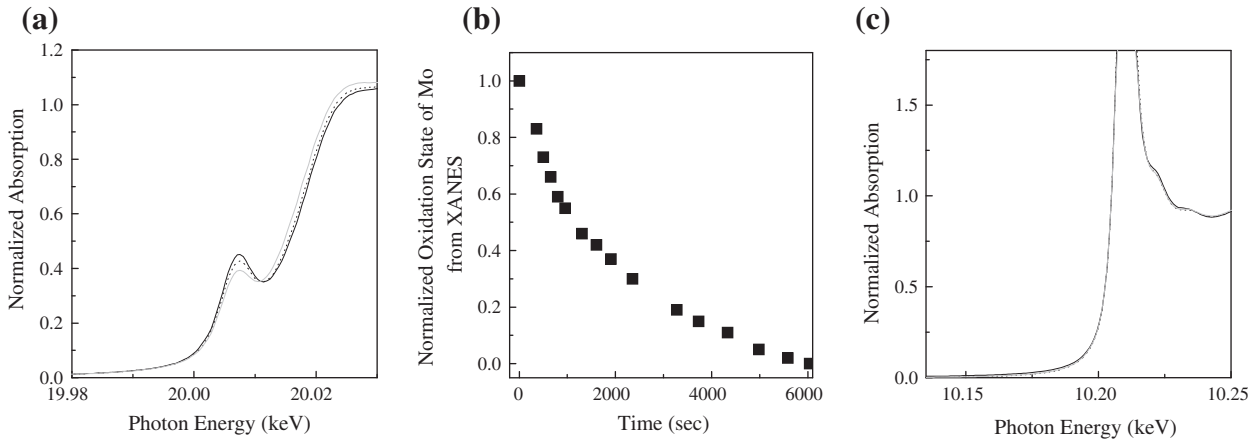

Fig. 6. (a) Mo K-edge XANES spectra over the 4Mo catalyst: in air at room temperature (—), under steady-state reaction with ethanol/O_2 at 453 K (- - -), and after 60 min of anaerobic titration at 453 K (▬). (b) Normalized oxidation state for the 4Mo catalyst during anaerobic titration. The normalized oxidation state of Mo is defined to be 1 under steady-state reaction conditions and 0 at the end of 60 min of anaerobic titration. (c) W LIII-edge XANES spectra during anaerobic titrations using ethanol over the 4W catalyst: in air at room temperature (—), under steady-state reaction with ethanol/O_2 at 453 K (- - -) and after 60 min of anaerobic titration at 453 K (▬).

gen atom between two metal atoms (M—O—M), and the bridging oxygen atom between the metal atom and the support (M—O—S) [50]. Previous studies using Raman spectroscopy have shown that changes in surface structure that occur with an increase in surface density up to monolayer coverage result in a transition from monomeric to polymeric species [43,51]. This results in an increase in the number of bridging oxygen atoms (on a per metal atom basis) while the number of terminal oxygen atoms remains constant. Thus, anaerobic titrations suggest that the terminal M=O oxygen is not the active oxygen site removed during acetaldehyde formation, as their density does not vary with surface density. Rather, oxygen in either M—O—M or M—O—S species function as active redox sites.

3.5. X-ray absorption characterization

The molecular identity of the active oxygen species was further probed by characterizing catalysts that had undergone anaerobic titration with in situ X-ray absorption spectroscopy. X-ray absorption near edge spectroscopic (XANES) studies were used to quantify the oxidation state of Mo in the supported MoO_x catalysts during steady-state ethanol oxidation reactions and anaerobic titrations. Mo—K-edge XANES spectra were collected for the 4Mo catalyst under ambient conditions, steady-state ethanol oxidation reaction, and after 60 min of anaerobic titration. Results are shown in Fig. 6. The position of the absorption edge is a function of the oxidation state of the central metal atom. The absorption edge shifts to lower photon energies upon reaction and site titration, indicating that the catalyst undergoes reduction during reaction and that reduction increases during anaerobic titration, confirming observations from UV–vis absorption spectroscopy. The absorption edge was fit using a linear combination of the absorption spectra under steady-state conditions, and the absorption spectra were obtained after 60 min of anaerobic titration (Fig. 6b) to represent a normalized oxidation state of Mo in the catalyst, where the oxidation state of Mo is considered to be 1 (oxidized) under steady-state reaction conditions and 0 (completely reduced) at the end of 60 min of the titration, after which no further changes were observed (spectra were collected for an extra 4 min). This normalized oxidation state changes exponentially with time and correlates with the trend observed in the acetaldehyde production rate (shown in Fig. 5a) as a function of time during anaerobic titration. The timescales for the two do not match exactly since experimental conditions (gas flow and catalyst weight) were not replicated identically at the beamline. The XANES spectra in the final oxidation state can be fit with the absorption edges for MoO_2 and MoO_3 to obtain a final oxidation state of ~5.6, which is lower than what one would expect from the anaerobic titrations. This is attributed to non-ideal flow conditions in the XAS sample cell, possibly resulting in some by-passing of the pellet, which would lead to a smaller fraction of the catalyst to be reduced in comparison with titrations using a more ideal plug-flow reactor. In contrast to the 4Mo catalyst, the position of the W-LIII absorption edge for the 4W catalyst changes neither during reaction nor after anaerobic titration, as shown in Fig. 6c, and is representative of the predominantly acidic character of the catalyst and its resistance to reduction.

Extended X-ray absorption fine structure (EXAFS) spectra were collected on MoO_x—Al_2O_3 at the Mo—K edge before and after anaerobic titrations to elucidate changes in the local structure around the Mo atom during the anaerobic titration. Fig. 7a shows the magnitude of the Fourier transform of the EXAFS spectrum collected for an 8Mo catalyst before and after anaerobic titration. The magnitude, but not the bond position, decreases noticeably upon oxygen removal, indicating that a large number of O atoms are removed during the anaerobic titration for this catalyst. In comparison, the Mo-atom coordination and environment for the 0.5Mo catalyst (as shown by EXAFS in Fig. 7b) does not change after anaerobic titration, indicative of a low number of removable active oxygen atoms in this catalyst. This agrees with the values shown for the number of removable oxygen atoms per metal atom in Table 1.

A difference spectrum for the 4Mo catalyst calculated by subtracting a spectrum collected after ~120 min of anaerobic titration from a spectrum collected after ~3 min of anaerobic reaction was analyzed to gain further insight into the type of oxygen removed. The magnitude and the imaginary part of the Fourier transform of this difference spectrum for the 4Mo catalyst are shown in Fig. 8 and represent structural differences arising due to the removal of lattice oxygen during anaerobic titration. Fitting of this spectrum with phases and amplitudes associated with Mo—O bonds in Na_2MoO_4 then gives an estimate of the number and distance of O atoms removed. Na_2MoO_4 was chosen since $NaMoO_4$ has only one type of O atom at a fixed distance. Since a typical supported oxide catalyst comprises of a number of metal–oxygen bonds at different distances, fitting of the complete structure is difficult. Fitting of the difference spectra is simpler and ensures that only changes due to the reduction are being studied. Fitting results indicate that only one type of O atom is removed at a distance of

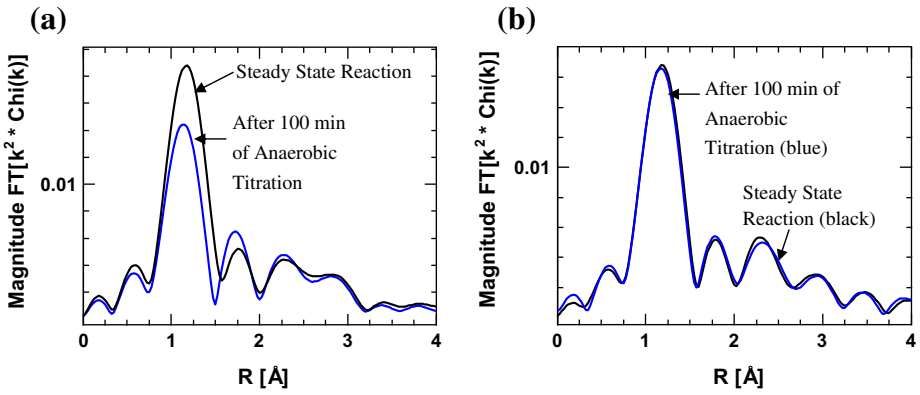

Fig. 7. Radial distributions from EXAFS spectra collected before and after anaerobic titration for the (a) 8Mo catalyst and (b) 0.5Mo catalyst.

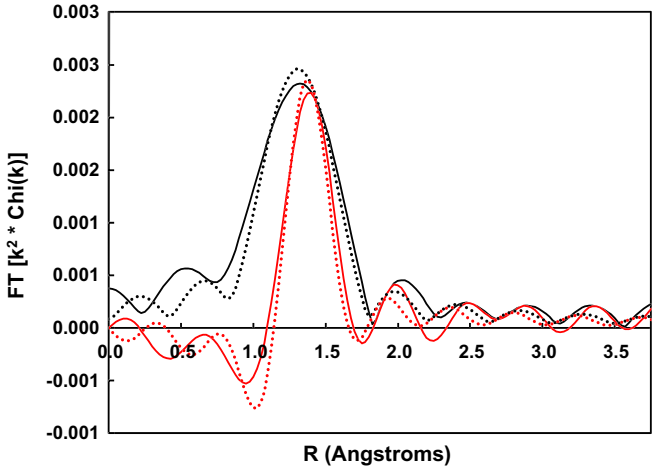

Fig. 8. Fourier transform of the difference spectrum calculated for the 4Mo catalyst during anaerobic titration. Curves were fit with the amplitude and frequency associated with Mo—O bonds (obtained by fitting the spectrum obtained for Na_2MO_4). The Fourier transform (FT) and the real part of the Fourier transform (RP of FT) are marked in the figure. The magnitude of the Fourier transform (black) and the imaginary part of the Fourier transform (red) are shown in the figure. Experimental data collected are shown as solid lines, and fitting is shown as dotted lines.

1.82 Å. This can then be compared to reference bond lengths obtained from MoO_3 using our previous XRD characterization of these catalysts [38]. Terminal Mo=O bond lengths in MoO_3 are ~1.6–1.8 Å [34,52] while bridging Mo—O—Mo bonds are ~1.8–2.0 Å. It is expected that the molybdenum–oxygen bond lengths in oxide domains would be different, but not significantly different from those in MoO_3. While the possibility of structural reorganization cannot be ignored, the fact that a good fit can be obtained with only one type of bond length suggests that only one type of oxygen atom is active for ethanol oxidation and will be supported by further evidence. The large bond lengths obtained by fitting tend to exclude the possibility of terminal Mo=O oxygen being this active species. It is possible that a number of O atoms at various distances are removed, but the good fit one can obtain by using only a single type of Mo—O bond is a strong indication that the method employed is a suitable one. Thus, anaerobic titration analysis during XAS indicates that there is a low probability of terminal Mo=O bonds being active redox sites in MoO_x—A_2O_3 catalysts.

3.6. Ethanol reactions probing the active oxygen site

In order to gauge the relative importance of oxygen atoms in M—O—M and M—O—Al sites (where M is a reducible metal atom), support effects on ethanol oxidation rates at 453 K were investigated using vanadium oxide catalysts supported on Al_2O_3, TiO_2, and CeO_2. Acetaldehyde formation rates and acetaldehyde selectivities are summarized in Table 2. Rates on bare supports are insignificant and thus allow for direct comparison of catalysts. The UV–vis absorption edge energies of these catalysts (shown in parenthesis in Table 2 along with catalyst name), and thus domain sizes, are nearly identical. Therefore, changes in rate are not expected to result from changes in domain size. Both the acetaldehyde formation rate per metal atom and product selectivity depend significantly on the support. CeO_2- and TiO_2-supported VO_x are more active and selective than Al_2O_3-supported VO_x. The support properties likely affect the availability and density of active and reducible oxygen atoms. Because these catalysts have the same VO_x domain size, active sites must be linked to the metal support in order to draw dependence from the support. Thus, this work points to metal–oxygen-support bridging oxygen atoms as active redox sites for acetaldehyde formation. A similar conclusion has been reached for supported V_2O_5 catalysts for the oxidation of propylene to acrolein, where the electronegativity of the support oxide cation was correlated to the propylene to acrolein turn-over frequency [53]. In fact, this has been used to modify the performance of SiO_2-supported vanadium and tungsten oxide catalysts by adding monolayers of TiO_2 on the SiO_2 and anchoring the active oxide on the TiO_2 [54]. However, based on our studies, it is not possible to discount the electronic effect of the support atom on the active metal atom from those effects on the availability of the Mo—O—Al oxygen atom. Attempts to measure active site densities on these catalysts were unsuccessful as TiO_2 and CeO_2 supports are themselves reducible during ethanol oxidation and results obtained thus far have been inconclusive.

Redox site densities were also quantified in binary MoO_x/WO_x—Al_2O_3 catalysts to investigate the kinetic relevance of oxygen atoms linking two metal atoms (M—O—M oxygen). Table 1 shows the redox sites per metal atom for binary MoO_x/WO_x—Al_2O_3 catalysts. In our previous studies [39], we have shown that the Mo and W oxides are well mixed in the 2Mo/2W catalyst and chemically segregated in the 0.5Mo/0.5W catalyst. Thus, in the 2Mo/2W catalyst, there should exist a large number of Mo—O—W linkages; the O availability in these linkages is expected to be different from both Mo—O—Mo and W—O—W. However, it is observed that the number of O atoms available per metal atom in this mixed binary oxide catalyst is the arithmetic mean of that available for the 2Mo catalyst and the 2W catalyst. Similarly, the O* density for the 0.5Mo/0.5W catalyst, where the linkages are predominantly still Mo—O—Mo and W—O—W, is the arithmetic mean of the 0.5Mo and 0.5W catalyst. This indicates that the change in the availability of the metal–oxygen–metal bridging oxygen does not have a

significant impact on the acetaldehyde formation rate and thus, is not expected to be the oxygen atom removed from the catalyst during ethanol oxidation to acetaldehyde. A similar conclusion was reached by Kim et al. [35], who demonstrated that the prevalence of V—O—V bonds in polymeric structures of VO_x—Al_2O_3 catalysts provided no enhancement in their activity for methanol ODH.

These studies thus indicate that metal—oxygen-support bridging oxygen atoms play a critical role in the formation of acetaldehyde from ethanol and are the catalytically active sites for ethanol oxidation, which has previously been demonstrated through theoretical calculations for methanol oxidation to formaldehyde [55]. As mentioned earlier, this synergy is possibly due to electronegativity of support metal atom relative to the supported oxide metal atom, which greatly influences the strength and hence availability of the oxygen atom linking the two.

3.7. Isotopic labeling kinetic studies

The rate-determining step in acetaldehyde formation has been shown to be an α-hydride elimination step [12,22] and was confirmed by quantification of isotope effects. Relative rates of acetaldehyde and ether formation over the 4Mo, 8V and 4W catalysts are shown using CD_3CD_2OH and CD_3CH_2OH with respect to CH_3CH_2OH in Table 3. Replacement of an α-H atom with a D-atom in ethanol results in a decrease in the acetaldehyde formation rate, whereas replacement of a β-H atom with a D-atom leads to no isotope effect. Thus, scission of a C—H bond in the CH_2 group of ethanol is the rate-determining step on Mo, W, and V oxide catalysts.

3.8. Analysis of ether formation mechanism

It is expected that acid products from ethanol dehydration would form through nucleophilic substitution reactions [56]. The two products that can be formed via nucleophilic substitution are the ether and the alkene. Table 4 shows the product selectivities during steady-state reaction in O_2/He at 543 K with different alcohols over an $Fe_2(MoO_4)_3$—MoO_3 catalyst, which we have shown has a comparable ODH selectivity to monolayer VO_x—Al_2O_3 catalysts for ethanol reactions [38]. With an increase in the alcohol hydrocarbon chain length for primary alcohols, the overall dehydration product selectivity increases marginally, while the relative selectivity of alkene to ether increases substantially. Diethyl ether is the exclusive acid product from ethanol, whereas butene is the exclusive acid product from 1-butanol. For a given alcohol (propanol or butanol), the presence of the hydroxyl at the secondary position leads to a marked increase in the overall dehydration product selectivity, with only propene and butene formed as acid products. Increasing hydrocarbon size (carbon number) in linear alcohols increases the stability of the carbocation formed after H-atom abstraction (the rate-determining step), and transitioning from primary to secondary to tertiary alcohols introduces greater steric hindrance toward a second reacting alkoxy required for ether formation. As shown previously using DRIFTS, the nonlinear dependence of ether formation rates on ethoxy coverage suggests that the rate-determining step for ether formation involves interaction between two adsorbed and presumably neighboring ethoxy species. An increase in carbon number promotes the probability of an S_N1 type nucleophilic substitution and the presence of —OH at the secondary or tertiary position degrades the probability of an S_N2 type nucleophilic [56]. These chemical phenomena and observations suggest that the predominant mechanism for alkene formation is via an S_N1 substitution reaction, while ether formation primarily occurs through a S_N2 mechanism.

Table 3
Relative oxidation rates of CD_3CD_2OH and CD_3CH_2OH over supported MoO_x (4Mo atoms/nm^2), VO_x (8V atoms/nm^2) and WO_x (4Mo atoms/nm^2) catalysts on alumina. Rates are expressed relative to those obtained for undeuterated ethanol – reaction conditions are maintained at 453 K with 0.5% alcohol, 1.5% oxygen, and balance He.

Catalyst	Rate CD_3CD_2OH/CH_3CH_2OH	Rate CD_3CH_2OH/CH_3CH_2OH
4Mo	0.55	0.99
8V	0.50	1.00
4W	0.53	1.00

Table 4
Ether and alkene product selectivities for C2—C4 alcohols over $Fe_2(MoO_4)_3$—MoO_3 (1.0 mol% alcohol, 3.0 mol% O_2, 15–40 mg of catalyst at 453 K). The only remaining product for each reaction is the corresponding aldehyde produced via ODH.

Reactant	Catalyst	Ether selectivity (%)	Alkene selectivity (%)
Ethanol	$Fe_2(MoO_4)_3$	0.7	0.0
1-Propanol	$Fe_2(MoO_4)_3$	0.4	2.8
2-Propanol	$Fe_2(MoO_4)_3$	0.0	36.0
1-Butanol	$Fe_2(MoO_4)_3$	0.0	4.0
2- Butanol	$Fe_2(MoO_4)_3$	0.0	81.0

3.9. Discussion and mechanism elucidation

Oxidation of ethanol and methanol has previously been used to classify metal oxides as acidic or basic. While some aspects of the mechanism for ethanol oxidation have been reported, this study focuses on a more complete understanding of the mechanism with an emphasis on understanding the catalyst properties that affect the formation of both acetaldehyde and diethyl ether from ethanol. Based on the studies outlined earlier, it is possible to outline a complete mechanism for ethanol oxidation as follows.

3.10. Adsorption of ethanol

The first step for both acetaldehyde and ether formation is the adsorption of ethanol as an ethoxy species, observed in the DRIFTS spectra collected during reaction and formed concurrently with protonation of, presumably, a terminal oxygen (O_T).

$$CH_3CH_2OH + M{=}O_T \overset{K_1}{\leftrightarrow} CH_3CH_2O{-}M{-}O_TH \quad (1)$$

3.11. Acetaldehyde formation

The next step in acetaldehyde formation is the rate-determining abstraction of an H atom from the ethoxy species and concurrent reduction of the catalyst surface via removal of a redox-active bridging lattice oxygen (O_B) in a Mars–van Krevelen redox mechanism. The catalyst is then immediately reoxidized using oxygen from the gas phase. Required steps are shown in Eqs. (2)–(6).

C—H bond scission

$$CH_3CH_2O{-}M{-}O_TH + O_B \overset{k_2}{\rightarrow} CH_3CHO{-}M{-}O_TH + O_BH \quad (2)$$

Acetaldehyde desorption

$$CH_3CHO{-}M{-}O_TH \overset{K_3}{\leftrightarrow} M{-}O_TH + CH_3CHO \quad (3)$$

Adsorption site regeneration

$$O_BH + M{-}O_TH \overset{K_4}{\leftrightarrow} M{=}O_T + H_2O_B \quad (4)$$

Loss of lattice oxygen

$$H_2O_B \overset{K_5}{\leftrightarrow} \blacksquare + H_2O_B \quad (5)$$

Reoxidation of the catalyst

$$\blacksquare + \frac{1}{2}O_2 \overset{K_6}{\leftrightarrow} O_B \quad (6)$$

3.12. Diethyl ether formation

For diethyl ether formation, the mechanism involves an S_N2 reaction between two adsorbed ethoxy species, as evidenced from the DRIFTS studies obtained during reaction and titration with water and the relative ether to alkene selectivities for different alcohols over the same catalyst. A similar mechanism has been proposed for Mg_yAlO_x catalysts [46]. Lattice oxygen is not removed during this reaction. Desorption of the products (ether and water) subsequently regenerates the adsorption sites. Mechanistic steps for DEE formation are shown in Eqs. (7)–(9).

Condensation of ethoxy species

$$2C_2H_5O{-}M{-}O_TH \overset{k_7}{\rightarrow} O_T{-}M{-}H_2O + (CH_3CH_2)_2O{-}M{-}O_T \quad (7)$$

Ether desorption

$$(CH_3CH_2)_2O{-}M{-}O_T \overset{K_8}{\leftrightarrow} (CH_3CH_2)_2O + M{=}O_T \quad (8)$$

Water desorption

$$O_T{-}M{-}H_2O \overset{K_9}{\leftrightarrow} M{=}O_T + H_2O \quad (9)$$

Nomenclature for Eqs. (1)–(9).
M represents a metal site;
O_T represents a terminal oxygen;
O_B represents a bridging oxygen;
■ represents a vacancy.

These mechanisms can be used to obtain rate expressions for product formation rates. The rate of production of acetaldehyde is then given by

$$r_{AC} = k_2[CH_3CH_2O{-}M{-}O_TH][O_B]z/[O_B]_{Total} \quad (10)$$

where $[O_B]_{Total}$ represents the total number of bridging oxygen atoms (based on stoichiometry) and $z/[O_B]_{Total}$ represents the probability of an ethoxy species being adjacent to a removable bridging oxygen.

This can be modified to

$$r_{AC} = \frac{k_2[CH_3CH_2O{-}M{-}O_TH][O_B]_z}{[O_B]_{Removable\ Total}} * \frac{[O_B]_{Removable\ Total}}{[O_B]_{Total}} \quad (11)$$

here $[O_B]_{Removable\ Total}$ represents the total number of removable bridging oxygen atoms, which is measured by the anaerobic titration.

The rate of ether formation can be written as

$$r_{DE} = \frac{k_7[CH_3CH_2O{-}M{-}O_TH]^2 z_2}{[M{=}O_T]_{Total}} \quad (12)$$

where $[M{=}O_T]_{Total}$ represents the total number of metal adsorption sites and $z_2/[M{=}O_T]_{Total}$ represents the probability of an ethoxy species being adjacent to another ethoxy species.

Site balances can then be written for metal adsorption sites and removable oxygen sites, as has been shown by Vannice [57] for a Mars–van Krevelen redox mechanism.

$$[M{=}O_T]_{Total} = [M{=}O_T] + [CH_3CH_2O{-}M{-}O_TH] + [(CH_3CH_2)_2O{-}M{-}O_T] + [CH_3CHO{-}M{-}O_TH] + [O_T{-}M{-}H_2O] \quad (13)$$

$$[O_B]_{Removale\ Total} = [O_B] + [O_BH] + [H_2O_B] + [\blacksquare] \quad (14)$$

Under steady-state conditions, the surface can be assumed to be saturated with ethoxy species and fully oxidized, yielding the following site balance equations.

$$[CH_3CH_2O{-}M{-}O_TH] = \frac{\lfloor M{=}O_T \rfloor_{Total}}{\{1 + K_1[CH_3CH_2OH]\}} \quad (15)$$

$$[O_B] = [O_B]_{Removable\ Total} \quad (16)$$

The steady-state rates then reduce to

$$r_{AC} = k_2[O_B]_{Removable\ Total} \quad (17)$$

$$r_{DE} = k_7[M{=}O_T]_{Total} \quad (18)$$

Predictions based on these mechanisms are found to match with all previously described experimental observations and rate dependencies, as shown in Table 5.

Thus, the proposed mechanism seems to capture all the dependencies observed experimentally and represents a possible mechanism for ethanol oxidation over supported metal oxide catalysts. This knowledge of the mechanism can now be used to understand what catalytic properties determine whether the catalyst is acidic or redox in nature. As explained earlier, the redox rate of a supported metal oxide catalyst is presumed to be determined by the number of removable oxygen linking the active metal atom to the support atom – it is expected that the electronegativities of these two atoms would determine the availability of the oxygen atom linking the two and hence, the number of active redox sites on the catalyst. Thus, the redox activity of a supported metal oxide catalyst can be tuned by varying the support linkages. The rate of ether formation, which proceeds through a nucleophilic substitution, depends on the electronegativity of the metal atom, which would determine the degree of electron deficiency of the C atom (in the CH_2 group) linked to the O atom in the adsorbed ethoxy species. Clearly, the two reaction pathways are not independent of each other – the electronegativity of the active metal atom is important for both products and results in interplay between the two product formation pathways.

4. Conclusions

Mechanisms were proposed for the formation of acetaldehyde and diethyl ether from ethanol over alumina-supported tungsten, vanadium, and molybdenum oxides. Ethanol adsorbs on the metal oxide as an ethoxy species, and this forms the intermediate for both acetaldehyde and ether formation. Acetaldehyde formation

Table 5
Comparison of mechanism predictions with experimentally observed dependencies.

Parameter	Experimentally observed (predicted by mechanism)
Steady-state ethanol conversion – ethanol reaction order	0 (0)
Steady-state ethanol conversion – oxygen reaction order	0 (0)
Acetaldehyde formation rate – dependence on ethoxy coverage	Linear (linear)
Acetaldehyde formation rate – dependence on removable lattice oxygen	Linear (linear)
Acetaldehyde formation rate – dependence on surface density	Zero (zero)
Ether formation rate – dependence on ethoxy coverage	Non-linear (second order)

rates depend linearly on ethoxy coverage while ether formation rates show a non-linear dependence on ethoxy coverage – acetaldehyde formation thus involves a single ethoxy species while the condensation of two ethoxy species is required for ether formation. Acetaldehyde formation requires the removal of an O atom from the catalyst surface, which was determined from kinetic and X-ray absorption analysis to be the oxygen atom linking the active metal atom to the support. While the electronegativity of the active metal atom is important for both acetaldehyde formation and ether formation, the support atom electronegativity plays a role in the availability of lattice oxygen for acetaldehyde formation. This provides a foundation for the choice of both the active metal oxide and the support to tune the catalytic properties of these extremely versatile supported metal oxide catalysts.

Acknowledgments

Partial support for this work was provided by NSF (CBET Career Award #0644707) and Purdue University. H. Nair was supported by the Bilsland Dissertation Fellowship at Purdue University. Acknowledgment is made to the Donors of the American Chemical Society Petroleum Research Fund for partial support of this research. Synchrotron beamtime was supported by Argonne National Labs GUP #8603. The use of the Advanced Photon Source (APS) was supported by the U.S. Department of Energy, Office of Science, Office of Basic Energy Sciences, under Contract No. DE-AC02-06CH11357. Materials Research Collaborative Access Team (MRCAT, Sector 10 ID) operations are supported by the Department of Energy and the MRCAT member institutions.

References

[1] L.J. Burcham, L.E. Briand, I.E. Wachs, Langmuir 17 (2001) 6164–6174.
[2] L.J. Burcham, L.E. Briand, I.E. Wachs, Langmuir 17 (2001) 6175–6184.
[3] L.J. Burcham, M. Badlani, I.E. Wachs, J. Catal. 203 (2001) 104–121.
[4] J.L. Bronkema, D.C. Leo, A.T. Bell, J. Phys. Chem. C 111 (2007) 14530–14540.
[5] C.D. Baertsch, K.T. Komala, Y.H. Chua, E. Iglesia, J. Catal. 205 (2002) 44–57.
[6] M. Badlani, I.E. Wachs, Catal. Lett. 75 (2001) 137–149.
[7] G. Deo, I.E. Wachs, J. Catal. 146 (1994) 323–334.
[8] A. Gervasini, J. Fenyvesi, A. Auroux, Catal. Lett. 43 (1997) 219–228.
[9] H. Knözinger, K. Kochloefl, W. Meye, J. Catal. 28 (1973) 69–75.
[10] H. Liu, P. Cheung, E. Iglesia, Phys. Chem. Chem. Phys. 5 (2003) 3795–3800.
[11] S.T. Oyama, G.A. Somorjai, J. Phys. Chem. 94 (1990) 5022–5028.
[12] S.T. Oyama, W. Zhang, J. Am. Chem. Soc. 118 (1996) 7173–7177.
[13] J.M. Tatibouet, Appl. Catal. A 148 (1997) 213–252.
[14] W. Zhang, A. Desikan, S.T. Oyama, J. Phys. Chem. 99 (1995) 14468–14476.
[15] W. Zhang, S.T. Oyama, J. Phys. Chem. 100 (1996) 10759–10767.
[16] C.J. Machiels, A.W. Sleight, J. Catal. 76 (1982) 238–239.
[17] A.I. Biaglow, R.J. Gorte, S. Srinivasan, A.K. Datye, Catal. Lett. 13 (1992) 313–321.
[18] W.E. Farneth, R.H. Staley, A.W. Sleight, J. Am. Chem. Soc. 108 (1986) 2327–2332.
[19] W.E. Farneth, E.M. McCarron, A.W. Sleight, R. Stacey, Langmuir 3 (1987) 217–233.
[20] M.V. Martínez-Huerta, X. Gao, H. Tian, I.E. Wachs, J.L.G. Fierro, M.A. Bañares, Catal. Today 118 (2006) 279–287.
[21] J. Le Bars, A. Auroux, M. Forissier, J.C. Vedrine, J. Catal. 162 (1996) 250–259.
[22] B. Kilos, A.T. Bell, E. Iglesia, J. Phys. Chem. C 113 (2009) 2830–2836.
[23] V. Ermini, E. Finocchio, S. Sechi, G. Busca, S. Rossini, Appl. Catal. A 198 (2000) 67–79.
[24] H.X. Dai, L. Chen, T.D. Tilley, E. Iglesia, A.T. Bell, Nat. Gas Conversion VII (2004) 679–684.
[25] W.E. Farneth, F. Ohuchi, R.H. Staley, U. Chowdhry, A.W. Sleight, J. Phys. Chem. 89 (1985) 2493–2497.
[26] N. Pernicone, F. Lazzerin, G. Liberti, G. Lanzavecchia, J. Catal. 14 (1969) 293–302.
[27] J. Edwards, J. Nicolaidis, M.B. Cutlip, C.O. Bennett, J. Catal. 50 (1977) 24–34.
[28] J.S. Chung, C.O. Bennett, J. Catal. 92 (1985) 173–176.
[29] J.S. Chung, R. Miranda, C.O. Bennett, J. Catal. 114 (1988) 398–410.
[30] F. Klose, T. Wolff, H. Lorenz, A. Seidel-Morgenstern, Y. Suchorski, M. Piorkowska, H. Weiss, J. Catal. 247 (2007) 176–193.
[31] Y. Iwasawa, Y. Nakano, S. Ogasawara, J. Chem. Soc., Faraday Trans. 1 74 (1978) 2968–2981.
[32] T. Ono, H. Kamisuki, H. Hisashi, H. Miyata, J. Catal. 116 (1989) 303–307.
[33] H. Nair, C.D. Baertsch, J. Catal. 258 (2008) 1–4.
[34] K. Routray, L.E. Briand, I.E. Wachs, J. Catal. 256 (2008) 145–153.
[35] T. Kim, I.E. Wachs, J. Catal. 255 (2008) 197–205.
[36] E.I. Ross-Medgaarden, W.V. Knowles, T. Kim, M.S. Wong, W. Zhou, C.J. Kiely, I.E. Wachs, J. Catal. 256 (2008) 108–125.
[37] T. Kim, A. Burrows, C.J. Kiely, I.E. Wachs, J. Catal. 246 (2007) 370–381.
[38] J.E. Gatt, H. Nair, C.D. Baertsch, Appl. Catal. B: Env. 99 (2010) 127–134.
[39] H. Nair, M.J. Liszka, J.E. Gatt, C.D. Baertsch, J. Phys. Chem. C 112 (2008) 1612–1620.
[40] C.D. Baertsch, M.A. Schmidt, K.F. Jensen, Chem. Commun. (2004) 2610–2611.
[41] M.D. Argyle, K. Chen, C. Resini, C. Krebs, A.T. Bell, E. Iglesia, J. Phys. Chem. B 108 (2004) 2345–2353.
[42] G. Centi, Selective Oxidation by Heterogeneous Catalysis, Kluwer Academic, New York, 2001.
[43] H. Hu, I.E. Wachs, S.R. Bare, J. Phys. Chem. 99 (1995) 10897–10910.
[44] J.C. Edwards, R.D. Adams, P.D. Ellis, J. Am. Chem. Soc. 112 (1990) 8349–8364.
[45] J.A.R. Van Veen, P.A.J.M. Hendriks, E.J.G.M. Romers, R.R. Andrea, J. Phys. Chem. 94 (1990) 5275–5282.
[46] E. Hillerová, H. Morishige, K. Inamura, M. Zdrazil, Appl. Catal., A 156 (1997) 1–17.
[47] X. Gao, J.-M. Jehng, I.E. Wachs, J. Catal. 209 (2002) 43–50.
[48] B.M. Weckhuysen, R.A. Schoonheydt, Catal. Today 49 (1999) 441–451.
[49] D.G. Barton, M. Shtein, R.D. Wilson, S.L. Soled, E. Iglesia, J. Phys. Chem. B 103 (1999) 630–640.
[50] J.L.G. Fierro, Metal Oxides: Chemistry and Applications, CRC Press, Boca Raton, FL, 2006.
[51] I.E. Wachs, Catal. Today 27 (1996) 437.
[52] F.D. Hardcastle, I.E. Wachs, J. Raman Spectrosc. 21 (1990) 683–691.
[53] C. Zhao, I.E. Wachs, J. Catal. 257 (2008) 181–189.
[54] E.I. Ross-Medgaarden, I.E. Wachs, W.V. Knowles, A. Burrows, C.J. Kiely, M.S. Wong, J. Am. Chem. Soc. 131 (2008) 680–687.
[55] H.Y. Kim, H.M. Lee, H. Metiu, J. Phys. Chem. C 114 (2010) 13736–13738.
[56] R.T. Morrison, R.N. Boyd, Organic Chemistry, sixth ed., Prentice Hall, Boston, 1992.
[57] M.A. Vannice, Catal. Today 123 (2007) 18–22.